Local Thermal Degradation Behavior of Heterophasic Polypropylene Copolymers

Norio Manabe,[1] Yoshimitsu Yokota,[1] Hisayuki Nakatani,[2] Shoutarou Suzuki,[3] Boping Liu,[3] Minoru Terano[3]

[1]*Research and Evaluation Center, Sumitomo Wiring Systems Co., Ltd., 1820 Nakanoike, Mikkaiti, Suzuka-si, Mie 513-8631, Japan*
[2]*Department of Bioengineering and Chemistry, College of Environmental Engineering and Architecture, Kanazawa Institute of Technology, 7-1 Ohgiga-oka, Nonoichi, Ishikawa 921-8501, Japan*
[3]*School of Materials Science, Japan Advanced Institute of Science and Technology, 1-1 Asahidai, Tatsunokuti, Ishikawa 923-1292, Japan*

Received 2 August 2004; accepted 30 January 2005
DOI 10.1002/app.22058
Published online 30 January 2006 in Wiley InterScience (www.interscience.wiley.com).

ABSTRACT: Polypropylene (PP) impact copolymer is one of the heterophasic PP systems that is improved by rubber modification. Because the copolymer is a complicated polymer blend, which mainly consists of PP and ethylene–propylene rubber (EPR) components, the degradation behavior has hardly been studied. In this study, the thermal degradation of the copolymer was studied through direct observation by atomic force microscopy, which is a powerful tool for observing a local domain in a polymer blend. The degradation behavior was visually captured by the mapping of topological changes. Although the EPR phase was hardly degraded, the neighboring PP matrix was degraded selectively. The degradation behavior of the copolymer was found to be heterogeneous. © 2006 Wiley Periodicals, Inc. J Appl Polym Sci 100: 1831–1835, 2006

Key words: atomic force microscopy (AFM); degradation; poly(propylene) (PP); thermal properties

INTRODUCTION

The mechanical properties of polypropylene (PP) are frequently improved by rubber modification.[1–4] The PP impact copolymer is one of the heterophasic PP systems, a growing segment of the thermoplastic market, which includes sheets, automobile bumpers, and covering materials for electric wires. In contrast to homopolymer PP, the PP impact copolymer synthesis consists of an additional copolymerization of propylene and ethylene in a secondary reactor.[4] Therefore, the PP impact copolymer is produced either by the multistage copolymerization of propylene with ethylene or by the blending of PP with ethylene–propylene rubber (EPR) and polyethylene (PE) and shows biphasic or multiphase morphology, depending on the rubber and PE content. This complicated morphology is controlled by the variation of the secondary reactor conditions, and the final properties of the PP impact copolymer can include a wide range of characteristics for specific applications.

The main problem of the PP impact copolymer is that the prediction of its material life is difficult. The degradation behavior is complicated due to due to its multiple components and morphologies. From the viewpoint of chemical structure, PP has tertiary carbon atoms and is known to be very vulnerable to oxidative degradation under the influence of elevated temperatures and sunlight.[5–13] PE and EPR have relatively more oxidative stability because of chemical structures with fewer tertiary carbon atoms.[14,15] On the basis of this understanding, it seems that the degradation behavior of the PP impact copolymer can be predicted easily. However, the oxidative degradation is also affected by the morphology in the solid state. The oxidation of the semicrystalline polymer is initially confined to the amorphous phase.[9] Thus, it is thought that degradation starts in the ethylene–propylene copolymer parts, which mainly form an amorphous phase. Considering these contradictory tendencies, it is necessary to investigate the differences in the stability of each of the fractions, with the use of direct observation to catch the changes in morphology caused by degradation.

Direct observation of the phase-separation structure in rubber-modified PP is possible by atomic force microscopy (AFM).[2,4] AFM can directly reveal the aggregation of the rubber phase directly on microtomed surfaces. Information about changes in the aggregation accompanying the progress of degradation will be very useful for understanding the degradation behavior of heterophasic PP systems.

Correspondence to: M. Terano (terano@jaist.ac.jp).

TABLE I
Content and Molecular Weights of the XI and XS Fractions in the PP Impact Copolymer

Fraction	Content (wt %)	M_n	M_w/M_n
XI	91.7	79,000	3.5
XS	8.3	144,000	3.5

M_n = number-average molecular weight.

TABLE II
Sequence Distribution of XI and XS Fractions

Fraction	Triad sequence (mol %)[a]					
	EEE	EEP	PEP	EPE	PPE	PPP
XI	4.8	2.0	0.7	8.9	1.3	82.3
XS	17.3	23.0	9.4	12.7	22.4	15.2

[a] Determined by ^{13}C-NMR. E = ethylene sequence; P = propylene sequence.

In this study, the degradation stabilities of PP and the rubber component in the PP impact copolymer were investigated, and the effects of degradation on the structure, including the topology and morphology, in the PP impact copolymer were directly observed by AFM. Finally, we discuss the degradation behavior of the heterophasic PP system.

EXPERIMENTAL

Materials and sample preparation conditions

A pellet of the PP impact copolymer was commercially obtained. The weight-average molecular weight (M_w) was 4.5×10^5, the distribution was 5.6, and the ethylene content was 12.8 mol %. This impact copolymer was reprecipitated from a boiling xylene solution into ethanol and dried in vacuo at 60°C for 8 h; freeze grinding was then carried out with liquid nitrogen. The obtained fine powder (1 g) was stirred in xylene (1 L) at 30°C for 12 h and divided into soluble and insoluble parts, respectively. These were sufficiently dried in vacuo and used as samples.

For AFM observation, the pellet was used directly as a sample without purification.

Measurements

The molecular weight of the sample was determined by gel permeation chromatography (GPC; Senshu, SSC-7100, Suginami, Tokyo) with polystyrene gel columns (Tosoh, TSK-gel G3000HHR and G5000HHR, Minato, Tokyo) at 140°C with *o*-dichlorobenzene as a solvent.

The primary structure was determined by ^{13}C-NMR measurement with a Varian Gemini-300 spectrometer (Palo Alto, CA) at 120°C on 20% (w/v) solution in 1,2,4-trichlorobenzene. Benzene-d^6 was added as an internal lock, and hexamethyldisiloxane was used as an internal chemical shift reference.

The melting temperature (T_m) of the sample was determined by differential scanning calorimetry (DSC; Mettler DSC 820, Oota, Tokyo).The thermogravimetric analyses (TGAs) of the xylene insoluble (XI) and xylene soluble (XS) fractions were performed with a Mettler TG50 at 130°C for 20 h under an air atmosphere with a flow rate of 50 mL/min. The temperature of the thermogravimetric analyzer was calibrated with the Curie point of nickel as a reference.

The AFM measurements were carried out with a Scanning Probe Microscope (SPM) device (Jeol, JSPM-520 SPM, Akishima, Tokyo). We calibrated the instrument by scanning a calibration grid with precisely known dimensions. All scans were performed in air with commercial Si SPM tips for alternating current (AC) mode at 1500 Hz. Topology and phase imaging were performed simultaneously in AC mode at the fundamental resonance frequency of the noncontact Si cantilever with a constant scanning rate of 37.9 μm/s. To get a sample with a smooth surface suitable for AFM observation, the pellet of the PP impact copolymer was cut by an ultramicrotome at −100°C.

Thermal oxidative degradation

Thermal oxidative degradation was carried out in an oven. The sample was put into a small vial and was allowed to stand in the oven in air. In the heater, the vial was covered with a heating jacket to achieve effective heat transfer to the samples.

RESULTS AND DISCUSSION

The characteristics of the XS and XI fractions are summarized in Tables I and II. As shown in the tables, the XI fraction was the main fraction in the PP impact copolymer and was primarily composed of the PP component. The XS fraction, on the other hand, had a complicated composition that mainly contained ethylene–propylene copolymer, which formed a rubber phase in the impact copolymer.

Figure 1 shows the DSC curves of both samples. The

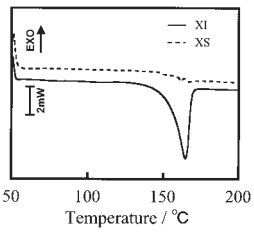

Figure 1 DSC thermograms of the XI and XS samples (heating rate = 20°C/min).

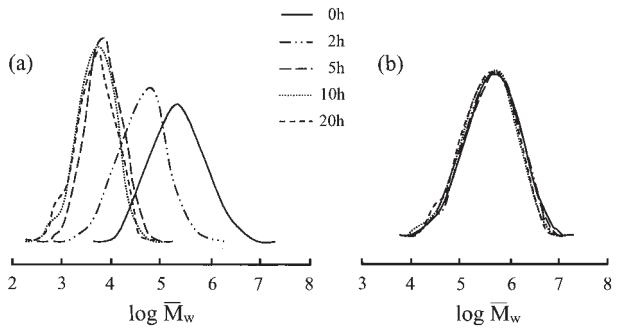

Figure 2 Degradation time dependences of GPC curves of the XI and XS samples (degradation temperature = 130°C).

XI fraction displayed a melting (endothermic) peak T_m at 165°C, and the XS fraction did not show any peaks, suggesting that it was amorphous.

Figure 2 shows the relationship between the time of thermal oxidative degradation and the change in the GPC curves in the XI and XS samples. At this degradation temperature, it was clear that the XI fraction was a semisolid, and the XS fraction was completely in a solution state. Considering the difference of oxygen permeability between the semisolid and solution state, the XS fraction might have been expected to be less stable due to a much higher oxygen permeability. However, a contrary result was actually obtained. In the case of the XI fraction, the GPC curves shifted to a lower molecular weight region with increasing degradation time, which meant that polymer chain scission was caused by the degradation. In contrast to the results for the XI fraction, the GPC curves of the XS fraction hardly changed with degradation time. TGA in isothermal conditions under an air atmosphere was performed, and the results are shown in Figure 3. The weight of the XS fraction was almost constant at 130°C for 20 h. On the other hand, the weight of the XI fraction increased after a pseudo-induction period, reached a maximum, and then decreased drastically. We suggest that the gradual increase in the weight of the XI fraction in the initial stage (up to ca. 7 h) was

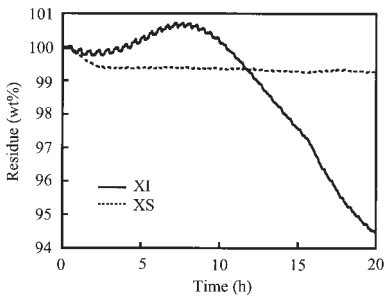

Figure 3 TGA of the XI and XS fractions at isothermal conditions (130°C, 20 h) under an air atmosphere with a flow rate of 50 mL/min.

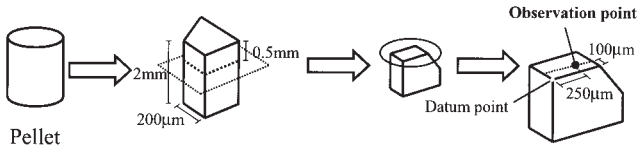

Figure 4 Schematic preparation of a sample for AFM observation and its observation point.

due to the predominant incorporation of oxygen into the polymer chains, accompanied by chain scission of tie molecules, whereas the significant decrease in the weight of the XI fraction in the later stage was caused by the formation of volatile fragments by dominant random chain scissions in the amorphous regions.[12] The thermogravimetry results show a significant difference in the thermal oxidation stability between the XS and XI fractions, which was consistent with the GPC results, as shown in Figure 2. The progress of degradation was suppressed by the existence of the ethylene unit.[14,15] It is thought that this suppression effect was larger than the difference in oxygen permeability.

These results indicate that the oxidative degradation of the PP impact copolymer was confined to the PP phase.

To gain access to the topology and morphology of heterogenic PP systems, such as the PP impact copolymer, and to do AFM analysis, it is convenient to use an ultramicrotome, which has a preparation technique well suited to obtaining a smooth surface for AFM analysis. Moreover, to study the changes in topology and morphology induced by degradation, it is necessary to observe the same point in one sample at different degradation times. To fulfill these requirements, the pellet was carefully cut and then tightly fixed to a planar plate with epoxy resin. The thermal oxidative degradation of one sample was performed with an oven for each required degradation time. The degraded sample was taken out of the oven for observation and then returned to the oven until the next required degradation time. To observe exactly same point, one corner of the sample edge was regarded as the datum point. As shown in Figure 4, all observations were performed at the point where the SPM tip progressed 250 μm in the longitudinal direction and 100 μm in the transverse direction from the datum point. The degradation time dependences of the topology and morphology were investigated by this unique technique.

Figures 5(a,b) shows AFM pictures of the topography and phase contrast images obtained from the PP impact copolymer. The dark areas in Figure 5(b) are separated soft phases assigned to the EPR part.[2,4] In the topography image, the dark portions correspond with submerged areas. According to Tanem et al.,[4] the height differences between the EPR phase and the matrix (PP) stem from differences in the expansion of each phase.

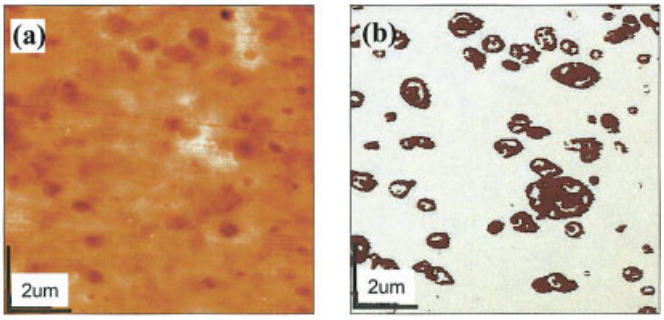

Figure 5 AFM images of a PP impact copolymer sample: (a) topography and (b) phase contrast images. [Color figure can be viewed in the online issue, which is available at www.interscience.wiley.com.]

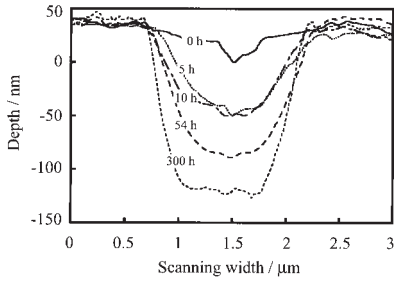

Figure 7 Topographic profiles of the EPR phase with different degradation times.

Figure 6 shows topographical pictures of one sample with several degradation times. Here, the term *degradation time* means integration time at the degradation temperature of 100°C, as described previously. This sample was scanned along the direction of the arrow at the circle position, denoted in Figure 6, to observe the change in topology. This circle position was the EPR phase. Figure 7 shows the overlapped profiles. The depth and width of the hole increased with increasing degradation time. The phase images for each degradation time of this EPR phase are shown in Figure 8. This phase had the form of an ellipse, with a major axis around 1 μm. Because its shape and size were mostly maintained after up to 300 h of degradation time, this EPR phase appeared to be barely affected by thermal oxidative degradation. This behavior was supported by the results for the XS sample characterized by the GPC and TGA methods and as shown previously in Figures 2 and 3. With these results considered, the growth of the hole was caused by the selective degradation of the PP interface. This revealed the interesting fact that a typical localization of oxidative degradation occurred in the PP impact copolymer.

Billingham and Vaillant et al.[9,10] reported that the localization of PP degradation is caused by the distribution of catalyst residue in the PP, which works as an initiator. The production process for the PP impact copolymers is a two-step polymerization method. In the first step, the propylene is polymerized; ethylene–propylene copolymerization is done in the following step. Thus, the catalyst residue is thought to be mainly located in the EPR phase produced by the second step. Although the EPR itself is much more stable in terms of thermal oxidative degradation, the neighboring PP

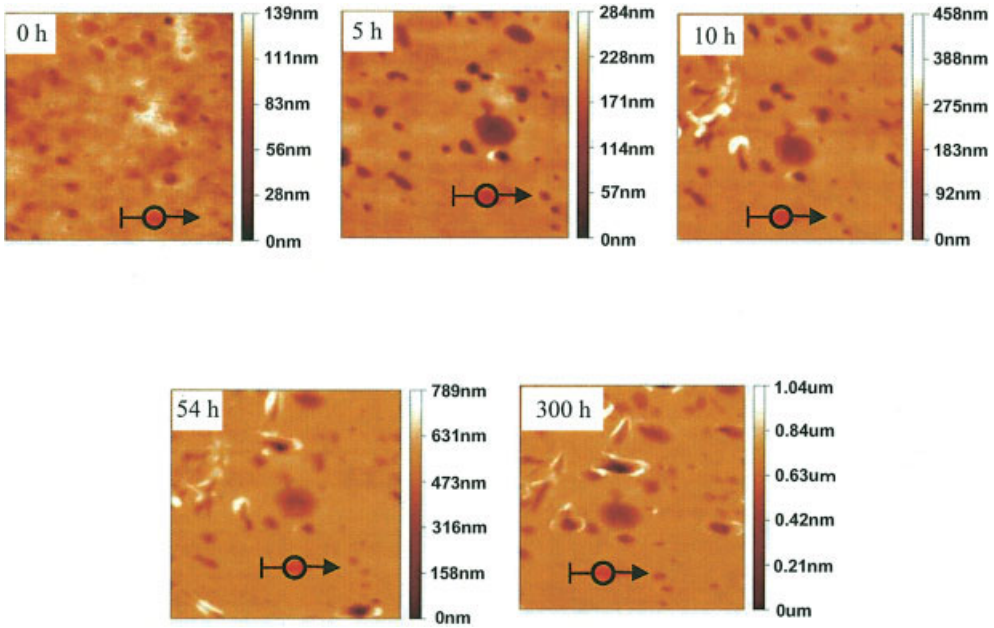

Figure 6 AFM topography images of one PP impact copolymer sample with different degradation times (degradation temperature = 100°C). [Color figure can be viewed in the online issue, which is available at www.interscience.wiley.com.]

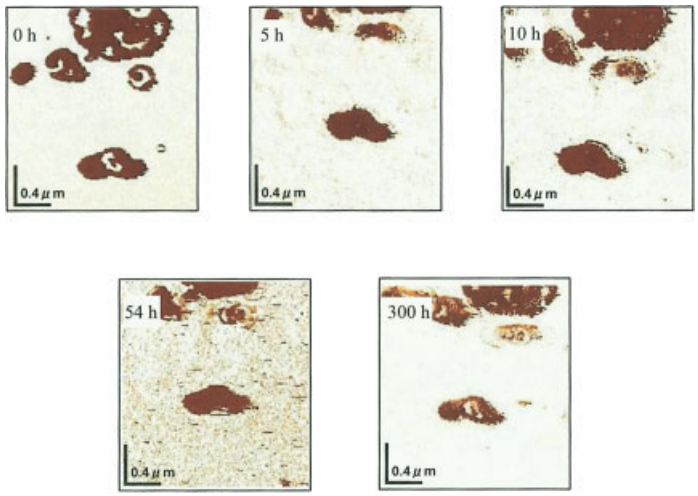

Figure 8 AFM phase contrast images of the EPR phase with different degradation times. [Color figure can be viewed in the online issue, which is available at www.interscience.wiley.com.]

matrix is affected by the existence of catalyst residue in the EPR phase. The heterogeneous behavior of degradation is associated with such a plausible location of catalyst residue.

CONCLUSIONS

The effect of thermal oxidative degradation on the topology of the PP impact copolymer was examined by the direct observation by AFM. We successfully applied the mapping of topological change to find that the degradation behavior of the PP impact copolymer was heterogeneous. Although the EPR phase was hardly degraded, the neighboring PP matrix was found to be degraded selectively.

References

1. Oksman, K.; Clemons, C. J Appl Polym Sci 1998, 67, 1503.
2. Tomasetti, E.; Legras, R.; Nysten, B. Nanotechnology 1998, 9, 305.
3. Lotti, C.; Correa, C. A.; Canevarolo, S. V. Mater Res 2000, 3, 37.
4. Tanem, B. S.; Kamfjord, T.; Augestad, M.; Lovgren, T. B.; Lundquist, M. Polymer 2003, 44, 4283.
5. Oswald, H. J.; Turi, E. J Polym Eng Sci 1965, 5, 152.
6. Kato, Y.; Carlsson, D. J.; Wiles, D. M. J Appl Polym Sci 1969, 13, 1447.
7. Carlsson, D. J.; Wiles, D. M. Macromolecules 1969, 2, 587.
8. Carlsson, D. J.; Wiles, D. M. Macromolecules 1969, 2, 597.
9. Knight, J. B.; Calvert, P. D.; Billingham, N. C. Polymer 1985, 26, 1713.
10. Billingham, N. C. Makromol Chem Macromol Symp 1989, 28, 145.
11. Vaillant, D.; Lacoste, J.; Dauphin, G. Polym Degrad Stab 1994, 45, 355.
12. Girois, S.; Audouin, L.; Delprat, P.; Verdu, J. Polym Degrad Stab 1996, 51, 133.
13. Goss, G. S. B.; Nakatani, H.; George, G. A.; Terano, M. Polym Degrad Stab 2003, 82, 119.
14. Alam, M. S.; Nakatani, H.; Ichiki, T.; Goss, G. S. B.; Liu, B.; Terano, M. J Appl Polym Sci 2002, 86, 1863.
15. Nakatani, H.; Ichiki, T.; Alam, M. S.; Liu, B.; Tobita, E.; Terano, M. Mater Life 2003, 15, 137.